CHEMISTRY
A EUROPEAN JOURNAL

ChemPubSoc Europe

DOI: 10.1002/chem.201204048

Tuning the Photoisomerization of a N^C-Chelate Organoboron Compound with a Metal−Acetylide Unit

Nan Wang, Soo-Byung Ko, Jia-Sheng Lu, Leanne D. Chen, and Suning Wang*[a]

Abstract: To examine the impact of metal moieties that have different triplet energies on the photoisomerization of B(ppy)Mes_2 compounds (ppy = 2-phenyl pyridine, Mes = mesityl), three metal-functionalized B(ppy)Mes_2 compounds, **Re-B**, **Au-B**, and **Pt-B**, have been synthesized and fully characterized. The metal moieties in these three compounds are $Re(CO)_3$(*tert*-Bu_2bpy)-(C≡C), $Au(PPh_3)$(C≡C), and *trans*-Pt-$(PPh_3)_2$$(C{\equiv}C)_2$, respectively, which are connected to the ppy chelate through the alkyne linker. Our investigation has established that the Re^I unit completely quenches the photoisomerization of the boron unit because of a low-lying intraligand charge transfer/MLCT triplet state. The Au^I unit, albeit with a triplet energy that is much higher than that of B(ppy)Mes_2, upon conjugation with the ppy chelate unit, substantially increases the contribution of the $\pi\rightarrow\pi^*$ transition, localized on the conjugated chelate backbone in the lowest triplet state, thereby leading to a decrease in the photoisomerization quantum efficiency (QE) of the boron chromophore when excited at 365 nm. At higher excitation energies, the photoisomerization QE of **Au-B** is comparable to that of the silyl–alkyne-functionalized B(ppy)Mes_2 (**TIPS-B**), which was attributable to a triplet-state-sensitization effect by the Au^I unit. The Pt^{II} unit links two B(ppy)Mes_2 together in **Pt-B**, thereby extending the π-conjugation through both chelate backbones and leading to a very low QE of the photoisomerization. In addition, only one boron unit in **Pt-B** undergoes photoisomerization. The isomerization of the second boron unit is quenched by an intramolecular energy transfer of the excitation energy to the low-energy absorption band of the isomerized boron unit. TD-DFT computations and spectroscopic studies of the three metal-containing boron compounds confirm that the photoisomerization of the B(ppy)Mes_2 chromophore proceeds through a triplet photoactive state and that metal units with suitable triplet energies can be used to tune this system.

Keywords: boron · chelates · isomerization · photochemistry · transition metals

Introduction

N^C-chelate organoboranes, such as B(ppy)Mes_2 (ppy = 2-phenyl pyridine, Mes = mesityl), have recently been found to display thermally reversible photoisomerization, thereby changing color from colorless or light yellow to deep blue or green on excitation by light.[1] This property affords new opportunities in organoboron-based photochromic materials. We have shown that, by varying the N^C-chelate ligands and substituents, the colors of the dark isomers and the photoisomerization quantum efficiency of this class of boron compounds can be tuned.[1,2] The key factors that have been found to have a great impact on the photoisomerization of the boron compounds are the charge-transfer (CT) transition from the mesityl groups to the chelate backbone and the steric congestion imposed by the mesityl groups.[2] For the photoisomerization to proceed efficiently, the lowest excited state must be dominated by the CT transition. As a result, extended π-conjugation of the chelate backbone, which leads to a low-lying $\pi\rightarrow\pi^*$ transition state, must be avoided.[3] Sterically bulky aryl groups, such as mesityl groups, around the boron center are necessary to enable the photoisomerization with moderate-to-high quantum efficiencies. We have also shown that the attachment of a Pt^{II} chelate unit onto the backbone can also greatly inhibit the photoisomerization process, owing to the introduction of a low-lying and highly emissive triplet state that effectively quenches the isomerization process.[1g] Nonetheless, the role of the triplet states in the photoisomerization of the N^C-chelate $BMes_2$ compounds was not understood until a recent report from our group, in which we demonstrated the possible involvement of a photoactive triplet state in the isomerization process[4] by examining the impact of triplet acceptors with various triplet energies that were covalently attached onto a N^C-chelate $BMes_2$ chromophore through a non-conjugated linker on the corresponding photoisomerization quantum efficiencies. A number of well-established photochromic chromophores, such as diarylethenes and spiropyrans,[5] are known to isomerize through photoactive triplet states.[6] The attachment of a transition-metal unit as a triplet sensitizer in such systems has been extensively used as an effective approach to modulate the isomerization effi-

---

[a] N. Wang, Dr. S.-B. Ko, J.-S. Lu, L. D. Chen, Prof. S. Wang
Department of Chemistry
Queen's University
Kingston, Ontario, K7L 3N6 (Canada)
Fax: (+1) 613-533-6669
E-mail: wangs@chem.queensu.ca

Supporting information for this article is available on the WWW under http://dx.doi.org/10.1002/chem.201204048.

ciency of the system.[7] To further understand the role of the triplet state and to determine whether transition-metal ions can be used as triplet sensitizers for the isomerization of N^C-chelate $BMes_2$ compounds, we initiated an investigation on the influence of Re^I ($[Re(CO)_3(tert\text{-}Bu_2bpy)]^+$), Au^I ($[Au(PPh_3)]^+$), and Pt^{II} metal units ($[Pt(PPh_3)_2]^{+2}$) on the isomerization of $B(ppy)Mes_2$ by using the general system shown in Scheme 1. These three metal units are chosen because of their distinct triplet energies and coordination geometries. We have found that these metal ions have a distinct impact on this system and the details are presented herein.

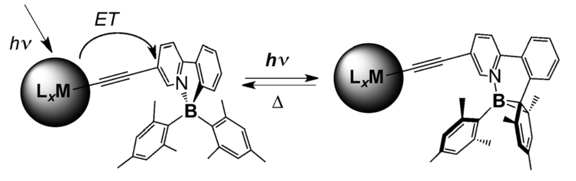

Scheme 1. Isomerization of N^C-chelate $BMes_2$ compounds with a metal–acetylide unit.

Results and Discussion

Synthesis and structures: The new metal-functionalized $B(ppy)Mes_2$ compounds were synthesized according to Scheme 2. The metal moiety was connected to the boron unit through an alkyne linker by using well-established procedures for related metal–acetylide compounds.[8,9] Parent boron molecule **B1** was obtained by the initial synthesis of **TIPS-B**, followed by the removal of the **TIPS** group according to literature procedures.[1b,c] By heating a mixture of $[Re(tert\text{-}Bu_2bpy)(CO)_3Cl]$, **B1**, $TlPF_6$, and Et_3N at reflux in THF, **Re-B** was obtained in moderate yield. **Au-B** and **Pt-B** were prepared by copper(I)-catalyzed transmetalation reactions between **B1** and the corresponding Au^I and Pt^{II} precursors, respectively. These complexes can be purified by column chromatography on silica gel. The Re^I and Pt^{II} complexes are air-stable, whereas the Au^I compound undergoes gradual degradation in air. All of these metal compounds were fully characterized by NMR spectroscopy, single-crystal X-ray diffraction, and elemental analysis.

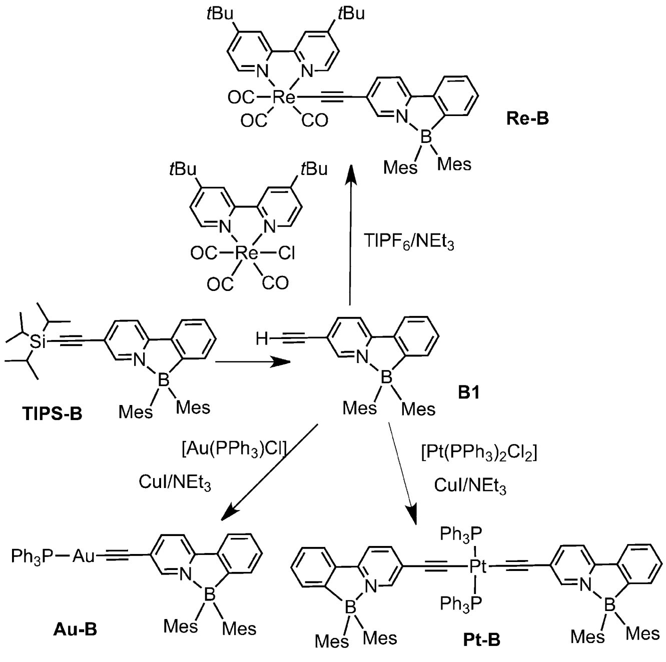

Scheme 2. Syntheses of N^C-chelate organoboron compounds with a metal–acetylide unit.

The crystal structures of these three metal complexes are shown in Figure 1, Figure 2, and Figure 3. Selected bond lengths and angles are given in Table 1. The metal ions in all three compounds display the expected geometry, that is, octahedral for Re^I, linear for Au^I, and square planar for Pt^{II}. The metal−P, metal−C, B−C, and B−N bond lengths in **Au-B** and **Pt-B** are very similar. Although the $B{-}C_{Mes}$ bond lengths in all three compounds are similar, the B−N bond (1.634(4) Å) in **Re-B** is significantly shorter than in **Au-B** (1.652(5) Å) and **Pt-B** (1.663(3) Å). This difference can be explained by the 18e Re^I unit, which takes less electron density away from the pyridyl ring of the N^C chelate com-

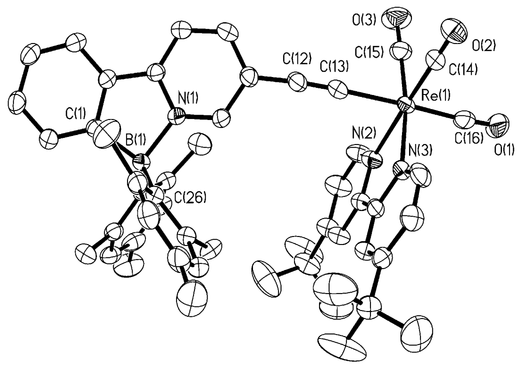

Figure 1. Crystal structure of **Re-B** with labeling schemes for selected atoms; thermal ellipsoids are set at 50% probability. Hydrogen atoms are omitted for clarity.

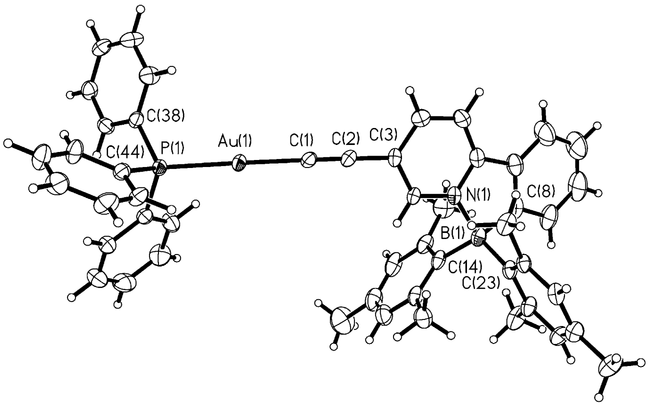

Figure 2. Crystal structure of **Au-B** with labeling schemes for selected atoms; thermal ellipsoids are set at 50% probability.

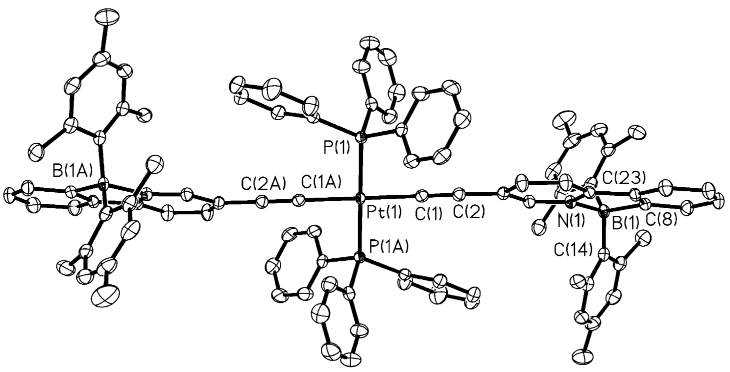

Figure 3. Crystal structure of **Pt-B** with labeling schemes for selected atoms; thermal ellipsoids are set at 50 % probability. Hydrogen atoms are omitted for clarity.

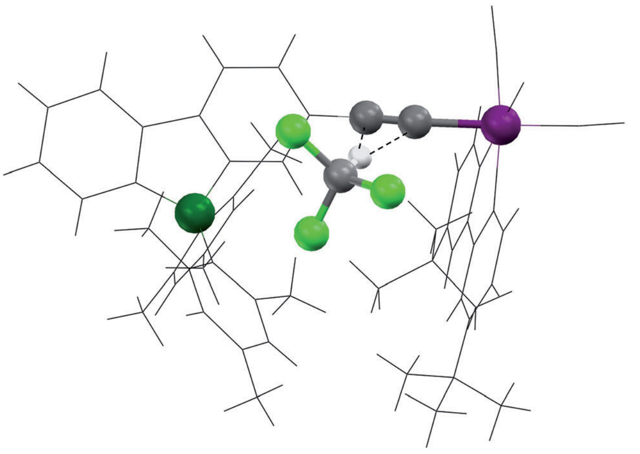

Figure 4. C−H⋯π interactions (about 2.50 Å) between $CHCl_3$ and the alkyne bond in **Re-B**.

Table 1. Selected bond lengths and angles of the metal complexes.

	Bond length [Å]				Bond angle [°]	
Re-B	Re(1)−C(14)	1.908(4)	Re(1)−C(13)	2.118(3)	C(16)-Re(1)-C(13)	172.63(16)
	Re(1)−C(15)	1.906(4)	Re(1)−N(3)	2.178(3)	C(15)-Re(1)-N(3)	171.85(13)
	Re(1)−C(16)	1.961(4)	Re(1)−N(2)	2.187(3)	C(14)-Re(1)-N(2)	170.88(14)
	B(1)−C(17)	1.657(5)	B(1)−C(1)	1.642(5)	N(1)-B(1)-C(1)	95.3(2)
	B(1)−C(26)	1.643(5)	B(1)−N(1)	1.634(4)	C(26)-B(1)-C(17)	115.1(3)
					Re-C(12)-C(13)	167.6(3)
Au-B	Au(1)−P(1)	2.2728(9)	Au(1)−C(1)	2.000(4)	C(1)-Au-P(1)	171.86(11)
	B(1)−C(14)	1.636(6)	B(1)−C(8)	1.638(6)	C(8)-B(1)-N(1)	95.3(3)
	B(1)−C(23)	1.655(6)	B(1)−N(1)	1.652(5)	C(14)-B(1)-C(23)	115.8(3)
					Au(1)-C(1)-C(2)	169.9(3)
Pt-B	Pt(1)−P(1)	2.3140(5)	B(1)−C(8)	1.633(3)	C(1)-Pt(1)-P(1)	87.69(6)
	Pt(1)−C(1)	2.002(2)	B(1)−C(14)	1.646(3)	C(1 A)-Pt(1)-P(1)	92.31(6)
	B(1)−C(23)	1.653(3)	B(1)−N(1)	1.663(3)	C(8)-B(1)-N(1)	95.58(15)
					C(14)-B(1)-C(23)	113.76(17)
					Pt(1)-C(1)-C(2)	176.80(19)

pared to the electron-deficient 14e Au^I unit and the 16e Pt^{II} unit. The other important feature as revealed from the crystal structure is that, in **Pt-B**, the two N^C-chelate units are coplanar and the π-conjugation is extended to the two alkyne linkers and the Pt^{II} atom, similar to the observations in some previously reported [*trans*-$Pt(PR_3)_2(acetylide)_2$] molecules.[13b,c] In **Re-B**, the three carbonyl ligands adopt a *facial* geometry, which is typical of $Re(CO)_3(bpy)X$ units,[8] to minimize the strong mutual *trans* effects of the carbonyl groups. The Re−C(16) bond length (1.961(4) Å) is significantly longer than those of the Re−C(14) and Re−C(15) bonds (1.908(4) and 1.906(4) Å, respectively), which can be attributed to the greater *trans* effect exerted by the alkyne ligand as compared to bpy. The M−C≡C bond angle in **Re-B** and **Au-B** is considerably distorted from linearity (167.6(3)° and 169.9(3)°, respectively). For **Re-B**, the proton of a $CHCl_3$ solvent molecule displays C−H⋯π interactions[10] with the alkyne bond, as evidenced by a H⋯C separation of about 2.50 Å, whereas, for **Au-B**, the H atoms of the phenyl ring from PPh_3 and the mesityl ring show C−H⋯π interactions with the alkyne bond, with a H⋯C separation in the range 2.90–3.00 Å (Figure 4 and Figure 5, respectively). Such interactions may be responsible for the bending of the M−C≡C bond in these two compounds. The chlorine atoms of the chloroform solvent molecules also form H-bonds with protons of the mesityl groups in the **Re-B** crystal lattice. For **Pt-B**, the most significant intermolecular interactions are π-stacking interactions between the ppy chelate units, with a shortest separation distance of 3.74 Å. As a result, molecules of **Pt-B** all orient along one direction, thereby forming an extended π-stacked lattice, as shown in Figure 6.

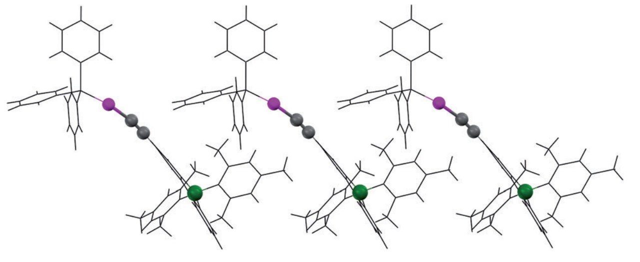

Figure 5. Relative orientations of the **Au-B** molecules and the C−H⋯π interactions (2.90–3.0 Å) in the crystal lattice.

Absorption spectra: All of the absorption spectra were recorded in degassed CH_2Cl_2 at room temperature. The data are shown in Table 2 and Figure 7. For comparison, the spectrum of **TIPS-B** is also shown in Figure 7. The absorption spectrum of **Re-B** can be assigned by comparison with previously known Re^I–α,α′-diimine complexes[11] and N^C-chelate four-coordinate boron complexes.[1] The absorption

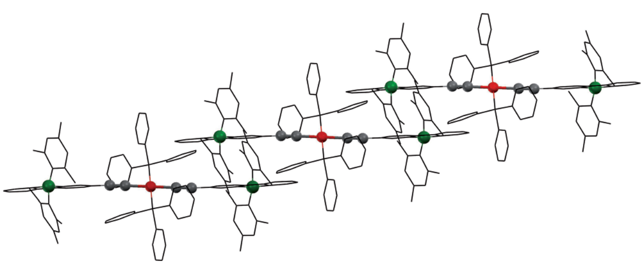

Figure 6. π-Stacking (shortest C···C separation distance is 3.74 Å) of **Pt-B** molecules in the crystal lattice. Hydrogen atoms are omitted for clarity.

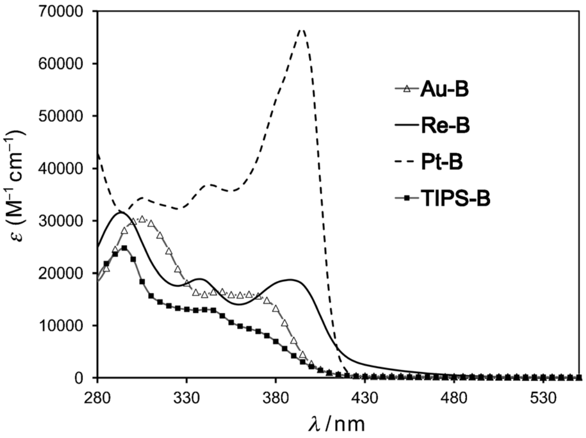

Figure 7. UV/Vis spectra of solutions of the metal complexes (ca. 1.0×10^{-5} M) in CH_2Cl_2 at ambient temperature.

band at 270–360 nm is attributed to a mixture of intraligand π→π* transitions centered on the diimine and alkynyl ligands. The low-energy absorptions at about 370–420 nm may be assigned to a mixture of charge-transfer transitions from the mesityl groups to the π-conjugated backbone and [d_π(Re)→π*(diimine)] metal-to-ligand charge-transfer (MLCT) transitions with moderate intensity. This enhanced MLCT transition can be explained by the incorporation of an acetylide ligand, which is known to raise the d–d state energy of the rhenium(I) center, thus enhancing the population of the MLCT state.[8] The absorption tail in the region 420–460 nm may be assigned to alkynyl→bpy charge-transfer transitions that are mixed with the MLCT transition.

The absorption spectrum of **Au-B** shows absorption bands in the regions 270–325 nm and 330–455 nm. By comparing these values to the absorption spectra of previously known Au^{I}–acetylide systems[12] and **TIPS-B**,[1d] the high-energy bands can be assigned to charge-transfer transitions from the alkyne to the PPh_3 ligand, whilst the low-energy bands can be attributed to charge transfer from the mesityl groups to the chelate backbone of the boron unit.

As in many previously reported Pt^{II}–phosphine–acetylide complexes,[13] **Pt-B** did not display any MLCT bands. Instead, an intense absorption band was observed at about 395 nm, which was assigned as a π→π* transition of the conjugated backbone that involves the two alkyne–B(ppy)Mes_2 units with contributions from the mesityl-to-chelate charge-transfer transitions. The strong absorption intensity and the red-shift of the absorption energy compared to those of **TIPS-B** and **Au-B** were clearly caused by the presence of two boron chromophores and by the extended conjugation of the backbone through the Pt^{II} center.

Luminescence spectroscopy: Luminescence spectra were recorded at room temperature and at 77 K for all of these complexes in degassed toluene (Figure 8). Upon excitation at 388 nm, **Re-B** displayed a broad, featureless emission peak at $\lambda_{max}=615$ nm at room temperature (Figure 8, top). By comparing to the spectra of previously reported Re^{I}–acetylide complexes,[11] this oxygen-sensitive orange–red emission is assigned as a ^{3}MLCT [dπ(Re)→π*(diimine)] transition (see the Supporting Information), as confirmed by the time-resolved phosphorescence spectrum (Figure 8, middle). At 77 K, **Re-B** shows bright luminescence at $\lambda_{max}=520$ nm (Figure 8, bottom). Because the emission spectrum has a very long decay lifetime and resolved vibrational features, this peak can be assigned as phosphorescence localized on the backbone of the **B1** unit. The dramatic blue-shift of the phosphorescent emission band from ambient temperature to 77 K may be explained by the high efficiency of the ^{3}π→π* emission of the alkyne–chelate backbone at 77 K, compared to the MLCT/CT phosphorescence of the Re^{I} unit.

At room temperature, **Pt-B** displays a dual emission at 480 and 520 nm upon excitation at 390 nm (Figure 8, top). Time-resolved phosphorescence spectroscopy (Figure 8,

Table 2. Photophysical data for the metal compounds.

	Absorption λ_{max} [nm] (ε [M^{-1}cm^{-1}])[a]	Emission λ_{max} [nm] (Φ[d]) 298 K[b]	77 K[c]	Phosphorescence decay lifetime [μs][e] 77 K[c]
Re-B	290 (31100), 335 (18800), 390 (18700)	615 (0.015)	520	2500 (1)
Au-B	305 (30400), 345 (16500), 370 (15700)	493, 500 sh (0.082)	493	1428 (1)
Pt-B	305 (34400), 345 (36700), 395 (66600)	452, 520 sh (0.015)	516	294 (1)
TIPS-B	295 (24800), 345 (12900), 375 (8090)	495 (0.42)[f]	482	–

[a] All of the spectra of solutions of the metal complexes (ca. 1.0×10^{-5} M) were recorded in degassed CH_2Cl_2 at ambient temperature. [b] All of the spectra of solutions of the metal complexes (ca. 1.0×10^{-5} M) were recorded in degassed toluene at ambient temperature. [c] All of the spectra of solutions of the metal complexes (ca. 1.0×10^{-5} M) were recorded in 2-methyltetrahydrofuran at 77 K. [d] A degassed solution of [*fac*-Ir(ppy)$_3$] in 2-methyltetrahydrofuran ($\Phi=0.97$)[14a] was used as a reference for quantum-efficiency measurements. [e] The decay lifetimes were obtained by fitting the decay curve with a single exponential function. [f] Determined by using 9,10-diphenylanthracene as a standard.[14b]

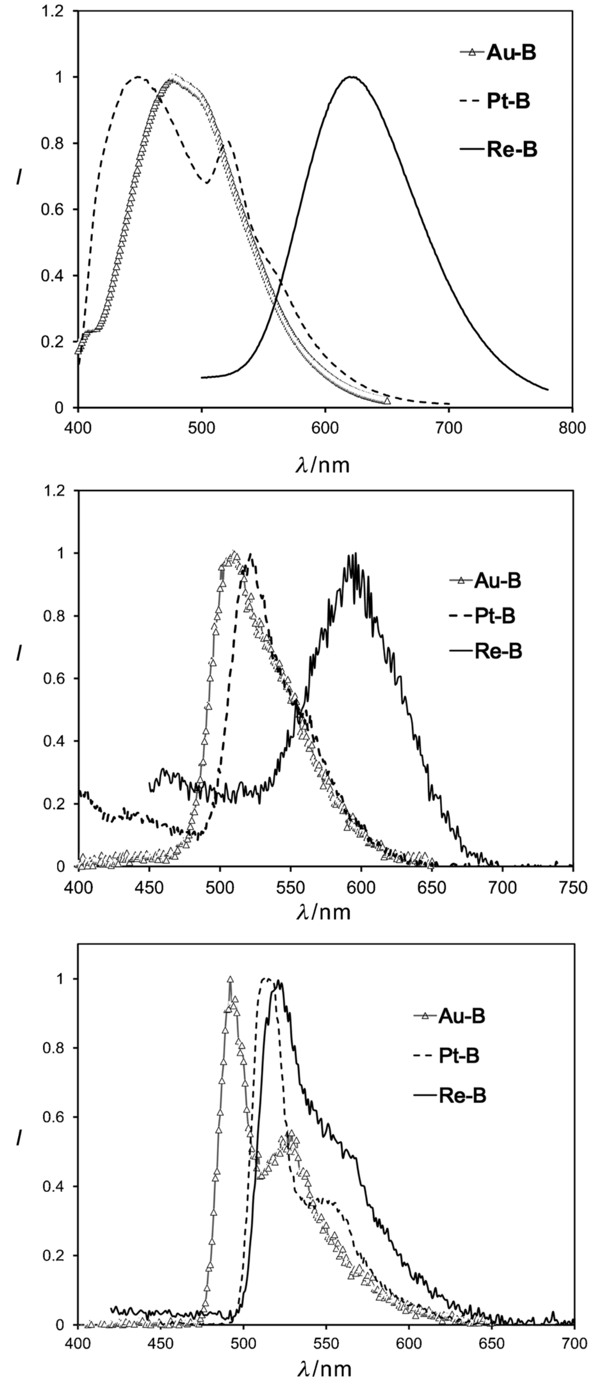

Figure 8. Top: Full emission spectra of solutions of **At-B**, **Pt-B**, and **Re-B** (ca. 1.0×10^{-5} M) in toluene at 298 K under a N_2 atmosphere. Middle: Time-resolved phosphorescence spectra of the metal compounds in toluene at 298 K under a N_2 atmosphere with a delay time of 140–160 μs. Bottom: Time-resolved phosphorescence spectra of the compounds in 2-methyltetrahydrofuran at 77 K with a delay time of 160–200 μs.

middle) and oxygen-sensitivity tests support the assignment of the peak at 520 nm as phosphorescence and the peak at 480 nm as fluorescence. Both peaks likely arise from transitions that involve the two conjugated B(ppy)Mes_2 units. At 77 K, **Pt-B** shows a phosphorescence emission peak at $\lambda_{max}=$ 516 nm, which resembles that of **Re-B** (Figure 8, top) and is assigned to the $^3\pi\rightarrow\pi^*$ transition that is localized on the conjugated backbone.

Upon excitation at 365 nm at ambient temperature, **Au-B** displays a broad emission band at 490 nm with a shoulder at about 500 nm (Figure 8, top). Time-resolved phosphorescence spectroscopy (Figure 8, middle) indicates that the band at 490 nm is fluorescence, whilst the shoulder band at about 500 nm is phosphorescence. By comparison with previously reported Au^I–acetylide complexes[12] and related boron compounds,[1] the fluorescence band may be assigned to a mesityl-to-chelate-backbone CT transition, whilst the phosphorescent band may be assigned to the alkyne–chelate backbone. At 77 K, the emission spectrum of **Au-B** resembles those of **Re-B** and **Pt-B**, with a very long decay lifetime (Figure 8, bottom), which is assigned as a π→π* transition that is localized on the conjugated backbone.

Photoisomerization: **Re-B** does not show any photoisomerization at all and remains intact after irradiation at 365 nm for more than 2 h, as shown by ^1H NMR spectroscopy (see the Supporting Information). The high photostability of **Re-B** can be attributed to a low-lying MLCT/CT state that involves the Re^I unit, which dominates the lowest excited state, as indicated by the absorption and phosphorescence spectra. Such a low-energy MLCT state can effectively quench the isomerization of the boron chromophore.

In contrast to the inactivity of **Re-B** upon excitation at 365 nm in toluene, **Au-B** undergoes rapid isomerization, thereby forming isomer **Au-B′** in quantitative yield and changing color from colorless to dark-blue, as shown in Figure 9. This photoisomerization process was monitored by ^1H and ^{31}P NMR and UV/Vis spectroscopy. The UV/Vis spectrum of **Au-B** shows a new, broad band at $\lambda_{max}\approx620$ nm upon irradiation, which is attributed to the **Au-B′** isomer. The ^1H NMR spectrum of **Au-B** in C_6D_6 shows that it under-

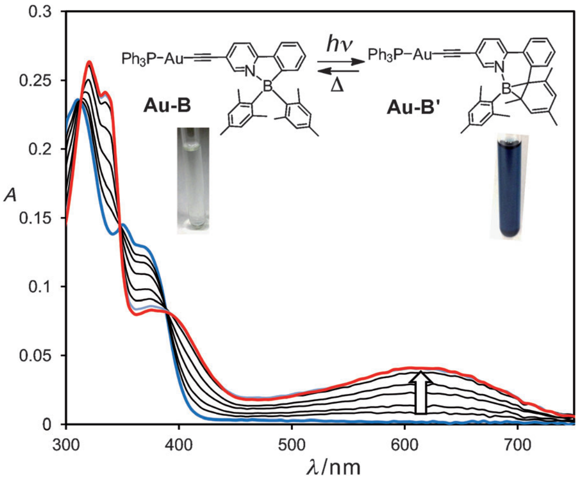

Figure 9. Changes in the UV/Vis spectra of **Au-B** (ca. 1.0×10^{-5} M) in toluene upon irradiation at 365 nm. Inset: Structures and colors of **Au-B** and its dark isomer, **Au-B′**.

goes clean conversion into **Au-B′** upon irradiation (see the Supporting Information). The structure of **Au-B′** is similar to that of the "dark isomer"[1a] of B(ppy)Mes$_2$, because of their similar and characteristic ^{1}H NMR spectra. The ^{31}P NMR spectra also confirmed the quantitative conversion of **Au-B** into **Au-B′** because it showed a distinct upfield shift of the ^{31}P signal of the phosphine group from $\delta = 42.96$ to 42.83 ppm (see the Supporting Information). This upfield shift of the ^{31}P signal is consistent with an increased electron density on the chelate backbone of the dark isomer,[1] which, in turn, increases the donation from the acetylide ligand to the Au^{I} center and decreases the donation from the phosphine ligand. The photoisomerization process of **Au-B** is fully thermally reversible, with an activation energy of 117 kJ mol^{-1}, similar to that[1a] observed for B(ppy)Mes$_2$ (see the Supporting Information).

The quantum yield[15] of the photoisomerization of **Au-B** at 298 K was determined to be about 0.46 on excitation at 365 nm, which was significantly less than those of B(ppy)-Mes$_2$ ($\Phi_{PI} = 0.85$)[1c] and **TIPS-B** (about 0.70). However, when excited at 310 nm, the photoisomerization quantum efficiency of **Au-B** greatly increased and the relative quantum efficiency ratio of **Au-B** to **TIPS-B** became about 1:1 (see the Supporting Information), which may be attributed to triplet-energy transfer from the Au^{I} unit onto the boron unit.

Pt-B was found to undergo photoisomerization upon irradiation at 365 nm in toluene. However, as shown in Figures 10 and 11, the change in the UV/Vis spectrum and the color of the solution is much less dramatic compared to that of **Au-B**, with a weak broad peak at $\lambda_{max} \approx 600$ nm. To establish whether both boron units are involved in the photoisomerization or not, we used ^{1}H NMR spectroscopy to monitor the process. As shown in Figure 11, upon irradiation, singlet proton H$_a$ ($\delta \approx 8.35$ ppm) was replaced with two new peaks, H$_b$ and H$_{b'}$, which maintained a 1:1 ratio and could be assigned to the isomerized and the non-isomerized boron chromophore, respectively. The single boryl-isomerization phenomenon can be explained by a fast intramolecular energy-transfer process in which the excited-state energy is absorbed by the isomerized boryl unit, owing to its low-energy absorption band, thus quenching the isomerization of the second boryl unit. The same phenomenon has also been observed in polyboron compounds that we reported earlier.[1c,e] The ^{31}P resonance of **Pt-B** also experiences a slight upfield shift from $\delta = 20.40$ to 20.34 ppm upon isomerization, as with **Au-B** (see the Supporting Information). The photoisomerization of **Pt-B** is very slow and much less efficient compared to **Au-B**, with a quantum yield of about 0.001. This low photoisomerization quantum efficiency may be attributed to the low-lying $\pi \rightarrow \pi^*$ state of the conjugated chelate backbone of the two B(ppy)Mes$_2$ unit.

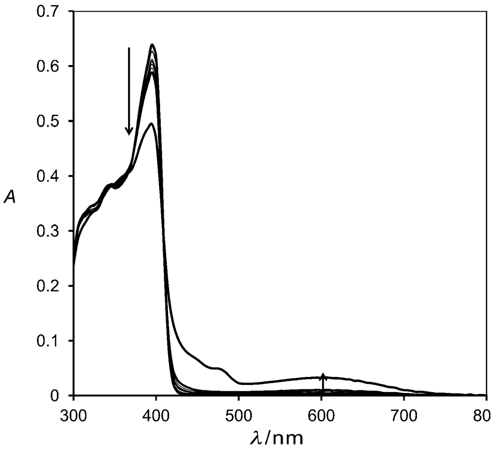

Figure 10. Changes in the UV/Vis spectra of **Pt-B** in toluene upon irradiation at 365 nm.

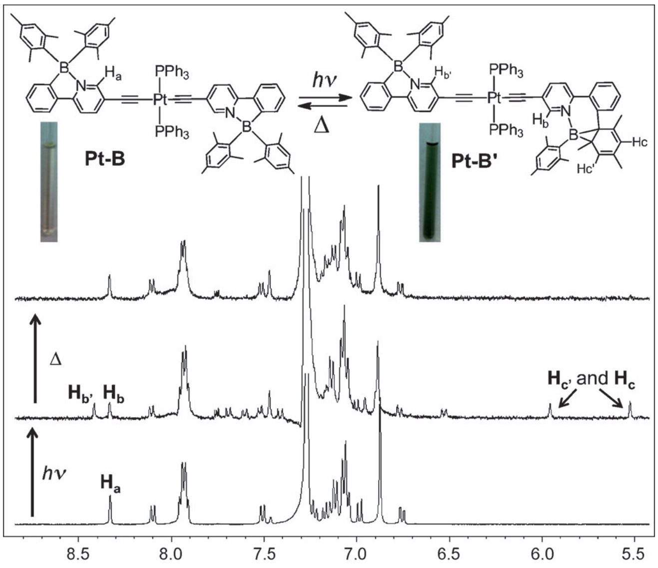

Figure 11. Bottom: Changes in the aromatic region of the ^{1}H NMR spectra of **Pt-B** in C_6D_6 upon UV irradiation under a N_2 atmosphere. Top: Colors of the solution and the structures of the compound before and after UV irradiation.

TD-DFT calculations: To gain a better understanding of the photophysical and photochemical properties of **Re-B**, **Au-B**, and **Pt-B**, TD-DFT computational studies were performed for all three compounds. In addition, we also performed calculations on Au(PPh$_3$)(C≡CH), *trans*-Pt(PPh$_3$)$_2$(C≡CH)$_2$, **TMS-B** (the analogue of **TIPS-B**), and B(ppy)Mes$_2$ to understand the impact of the metal component on the electronic properties of the boron chromophore. The data of the two lowest singlet excited states that have appreciable oscillator strengths and the lowest triplet state for all three metal compounds are provided in Table 3. The relevant molecular-orbital diagrams are shown in Figure 12. These TD-DFT results show that the S$_1$ energy of the metal compounds is much lower for **Re-B** compared to **TMS-B**, whilst it is somewhat higher for **Au-B** and **Pt-B**, which is in good agreement with the absorption spectra (Figure 8). The T$_1$ energy follows a similar trend, which agrees well with the observed

Table 3. TD-DFT results for **Re-B**, **Au-B**, and **Pt-B**.[a]

	State	Contribution (%)	Energy [eV]	λ [nm]	f[b]
Re-B	T_1	H→L (95)	2.01	617	–
	S_1	H→L (94)	2.04	608	0.0017
	S_2	H−3→L (15) H−2→L (74)	2.46	505	0.0328
Au-B	T_1	H−4→L (50) H→L (34)	2.61	474	–
	S_1	H→L (92)	2.89	429	0.0409
	S_2	H−1→L (87)	3.22	385	0.0041
Pt-B	T_1	H−9→L+1 (17) H−6→L (13) H−2→L (25) H→L (18)	2.63	471	–
	S_1	H−1→L+1 (36) H→L (62)	3.01	413	0.1180
	S_3	H−4→L (10) H−3→L+1 (37) H−2→L (44)	3.26	381	0.0507
TMS-B	T_1	H−4→L (40), H→L (51)	2.54	488	–
	S_1	H→L (97)	2.74	453	0.0253
	S_2	H−1→L (80)	2.99	415	0.0081
B(ppy)Mes$_2$	T_1	H−4→L (10) H→L (83)	2.75	450	–
	S_1	H→L (98)	2.89	430	0.0129
	S_2	H−1→L (79)	3.15	394	0.0067

[a] TD-DFT calculations were performed at the B3LYP level of theory by using the LANL2DZ basis set for the metal atoms and the 6-31G(d) basis set for all other atoms. [b] Oscillator strength.

phosphorescent spectra at ambient temperature (Figure 9, middle).

The key finding from the TD-DFT calculations of **Re-B** is that the S_1 and T_1 states are all charge-transfer transitions from π (involving orbitals from the chelate backbone, the alkyne bond, the CO ligand that is *trans* to the acetylide, and the Re atom) to π* (bpy), thus confirming the assignment of the lowest-energy absorption band and the ambient-temperature phosphorescence of **Re-B** to intraligand CT and MLCT transitions. In addition, the TD-DFT results indicate that the T_1 energy (2.01 eV) of **Re-B** is much lower than the triplet energy of the mesityl→chelate CT transition of the B(ppy)Mes$_2$ chromophore (about 2.70 eV), thus confirming that the photostability of the boryl chromophore in **Re-B** is indeed caused by the low lying intraligand CT/MLCT of the Re^{I} unit.

For **Au-B**, the S_1 state is a typical mesityl-to-alkyne–chelate charge-transfer transition with moderate oscillator strength, which is responsible for the lowest-energy absorption band and the fluorescence peak at ambient temperature. The T_1 state is dominated by a π→π* transition (HOMO−4→LUMO, 50%) of the alkyne–chelate backbone with about 34% mesityl→chelate CT transition, which is responsible for the observed phosphorescence peak of **Au-B**. Appreciable contributions from the Au^{I} atom are present in HOMO−4. The key difference between **TMS-B** (to simplify the computations, we calculated **TMS-B** instead of **TIPS-B**) and **Au-B** is the T_1 state. For **TMS-B**, the mesityl→chelate CT contribution to the T_1 state is much greater (51%) than the π→π* transition of the backbone (40%). Because the mesityl→chelate charge transfer is the key driving force of the photoisomerization, the greater Mes→chelate CT contribution to the T_1 state by **TIPS-B** compared to **Au-B** explains why, on excitation at 365 nm, the quantum efficiency of **Au-B** is lower than that of **TIPS-B**. The importance of the Mes→chelate CT transition in the T_1 state can be further illustrated by comparing the S_1 and T_1 states of **TMS-B** and B(ppy)Mes$_2$ in Table 3 and Figure 12. For the S_1 state, these two compounds have similar contributions from the Mes→chelate CT transition. However, for the T_1 state, the CT transition is 83% for B(ppy)Mes$_2$ and 51% for **TMS-B**, which is responsible for the higher photoisomerization quantum efficiency of B(ppy)Mes$_2$ (0.85) compared to that of **TIPS-B** (0.70). TD-DFT results indicate that the Au(PPh$_3$) unit contributes significantly to the higher triplet states (e.g., T_8, 3.55 eV; see the Supporting Information). Thus, the enhanced photoisomerization quantum efficiency of **Au-B** on excitation at 310 nm, as compared to that of **TIPS-B**, can be attributed to the triplet-state-sensitization effect exerted by the Au(PPh$_3$) unit.

For **Pt-B**, the S_1 state is dominated by the Mes→backbone CT transition, with high oscillator strength. However, the T_1 state is dominated by π→π* transitions that involve the conjugated backbone and significant contributions from the d orbitals of the Pt atom, as shown in Table 3 and Figure 12, which explains the low photoisomerization quantum efficiency of **Pt-B**. The dual-emission peaks at ambient temperature can be attributed to the S_1 and T_1 states.

For the individual components of compounds **Au-B** and **Pt-B**, TD-DFT computational results showed that the T_1 energies of Au(PPh$_3$)(C≡CH) (3.66 eV) and *trans*-Pt(PPh$_3$)$_2$(C≡CH)$_2$ (3.50 eV) were much higher than those of B(ppy)Mes$_2$ (2.75 eV), **TMS-B** (2.54 eV), and **B1** (2.56 eV). Therefore, in principle, connecting these metal components with the B(ppy)Mes$_2$ unit should enhance the photoisomerization quantum efficiency through triplet-state sensitization and energy transfer. The fact that the **Au-B** and **Pt-B** have either a lower or similar photoisomerization quantum efficiency, relative to that of the parent boron chromophore (**TIPS-B** or B(ppy)Mes$_2$), can be explained by the enhancement of the conjugation in the alkyne–boron chelate backbone by the metal unit, which lowers the energy of the π→π* transitions that are localized on the π-conjugated backbone, thus leading to a greater contribution of these transitions to the T_1 state and the partial quenching of the photoisomerization of the boron chromophore.

Conclusion

We have demonstrated that a metal–acetylide unit that is connected to the chelate backbone of the B(ppy)Mes$_2$ compound can have a significant impact on the photoactivity of the boron compound. The introduction of a Re(CO)$_3$(*tert*-Bu$_2$bpy) unit affords a low-energy MLCT/intraligand CT triplet state around the Re^{I} center, which can completely

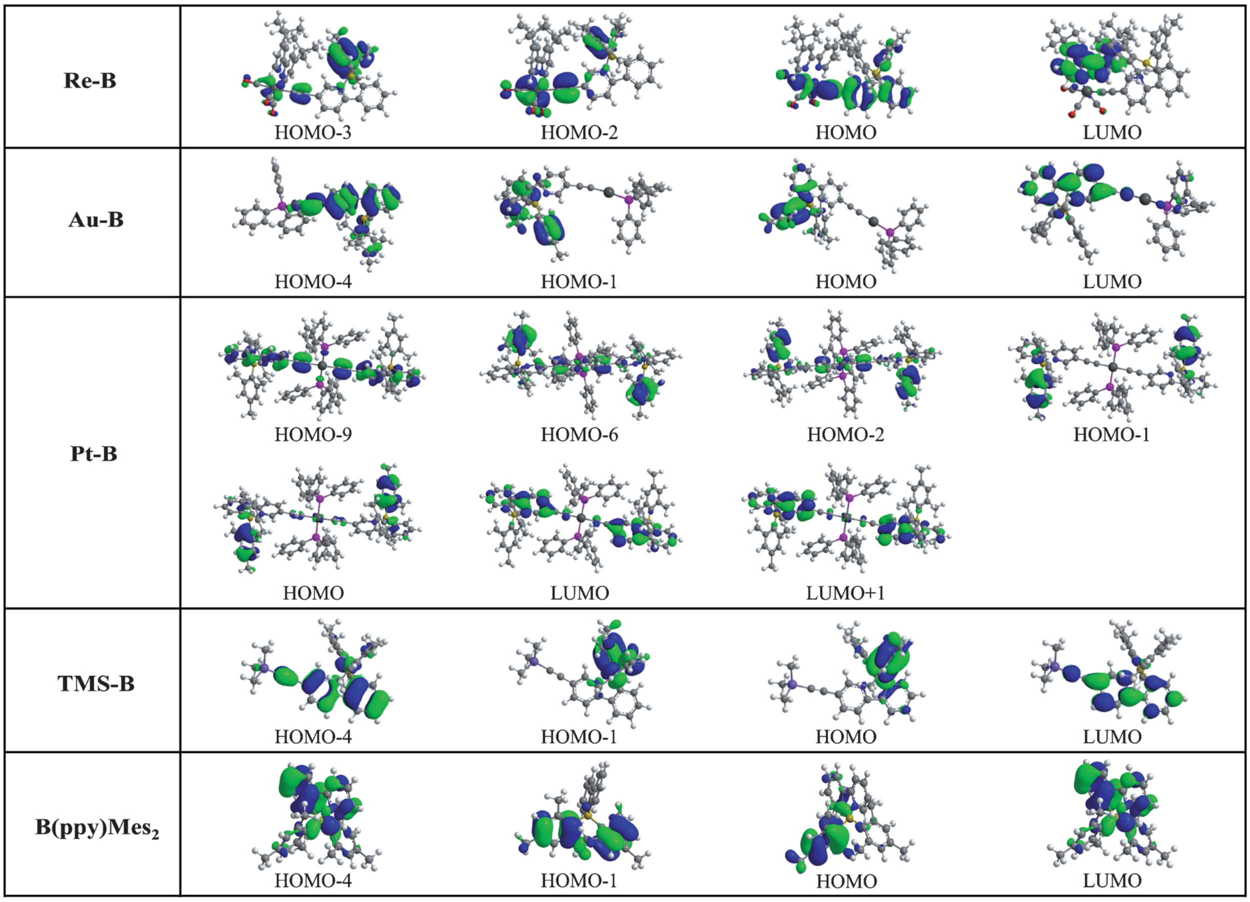

Figure 12. Isodensity surface plots for frontier orbitals of N^C-chelate $BMes_2$ compounds in the ground states (isodensity contour = 0.03).

shut off the photoactivity of the boron unit. The *trans*-Pt-$(PPh_3)_2(C{\equiv}CH)_2$ unit greatly enhances the π-conjugation of the chelate backbone of both boron units through the Pt center and the contribution of the π→π* transitions that are localized on the backbone to the T_1 state, thereby leading to a dramatic quenching of photoisomerization of the boron chromophore. The $Au(PPh_3)(C{\equiv}CH)$ unit also enhances the π-conjugation of the backbone and the contribution of the π→π* transitions of the backbone to the T_1 state, albeit to a much lesser extent. Thus, a significant decrease in the photoisomerization quantum efficiency of **Au-B** was also observed, compared to that of **TIPS-B**, when excited at the lowest-energy absorption band. At higher excitation energy, the photoisomerization quantum efficiency of **Au-B** becomes comparable to that of **TIPS-B** because of the triplet-state-sensitization effect. This study has established that the photoisomerization of $B(ppy)Mes_2$ indeed involves a photoactive triplet state. Furthermore, the CT transition from the mesityl groups to the chelate backbone must make a major contribution to the T_1 state to achieve efficient photoisomerization in this system. Finally, to use the metal units that have a high triplet energy as effective triplet sensitizers, π-conjugation between the metal unit, the linker, and the chelate backbone of the boron unit should be avoided.

Experimental Section

General procedures: All reactions were performed under a dry N_2 atmosphere by using standard Schlenk techniques unless otherwise noted. All starting materials were purchased from Aldrich Chemical Co. and used without further purification. Solvents were freshly distilled over appropriate drying reagents under a N_2 atmosphere. NMR spectra were recorded on a Bruker Avance 400 MHz spectrometer. Excitation and emission spectra were recorded on a Photon Technologies International QuantaMaster Model C-60 spectrometer. UV/Vis spectra were recorded on a Varian Cary 50 Bio UV/Vis spectrophotometer. Phosphorescent lifetimes were measured on a Photon Technologies International (PTI) phosphorimeter (Time-Master C-631F) that was equipped with a Xe flash lamp and a digital emission photon-multiplier tube at a band pathway of 5 nm for excitation and 2 nm for emission. Elemental analysis was performed at the Elemental Analysis Service, Department of chemistry, University of Montreal (Montreal, Quebec, Canada). Starting materials **B1**[8c] (Scheme 2) and [Re(*tert*-Bu_2bpy)$(CO)_3Cl$][8] were synthesized according to literature procedures.

Synthesis of Re-B: A mixture of [Re(*tert*-Bu_2bpy)$(CO)_3Cl$] (140 mg, 0.24 mmol), $TlPF_6$ (100 mg, 0.28 mmol), Et_3N (5 mL), and **B1** (150 mg, 0.35 mmol) in THF (100 mL) was heated at reflux under a nitrogen atmosphere for 2 days. Then, the insoluble inorganic salt was removed by filtration and the yellow filtrate was concentrated under vacuum. The residue was purified by column chromatography on silica gel (hexanes/CH_2Cl_2, 1:1) to give the analytically pure material. Recrystallization of the yellow product in $CHCl_3$/hexanes afforded the compound **Re-B** as yellow crystals (25 % yield). ^1H NMR (400 MHz, $CDCl_3$, 298.0 K): δ = 8.96 (d, J = 5.9 Hz, 2 H), 8.10 (s, 1 H), 8.08 (d, J = 1.7 Hz, 2 H), 7.66–7.61

(m, 4H), 7.47 (dd, $J=5.9$, 1.9 Hz, 2H), 7.20–7.13 (m, 2H), 6.56 (s, 4H), 2.15 (s, 6H), 1.63 (s, 12H), 1.46 ppm (s, 18H); $^{13}C\{^1H\}$ NMR (100 MHz, $CDCl_3$): $\delta=197.7$, 192.4, 164.6, 162.9, 155.6, 154.4, 152.8, 148.1, 145.9, 143.1, 140.2, 135.3, 134.7, 133.4, 130.8, 130.4, 129.5, 124.9, 124.2, 123.0, 120.8, 119.2, 116.3, 101.2, 35.5, 30.3, 24.7, 20.6 ppm; elemental analysis calcd (%) for $C_{52}H_{53}BN_3O_3Re$: C 64.72, H 5.54, N 4.35; found: C 64.58, H 6.17, N 3.99.

Synthesis of Au-B: A mixture of $[Au(PPh_3)Cl]$ (112 mg, 0.23 mmol), **B1** (100 mg, 0.23 mmol), CuI (2 mg), and Et_3N (6 mL) in degassed CH_2Cl_2 (30 mL) was stirred under a nitrogen atmosphere in the dark for 2 days. Then, the mixture was concentrated under vacuum and partitioned between CH_2Cl_2 and water. The aqueous layer was further extracted with CH_2Cl_2 (2×20 mL) and dried with $MgSO_4$. The crude mixture was further purified by column chromatography on silica gel (hexanes/CH_2Cl_2, 4:1) to give the gold(I) compound as a light-yellow powder (65% yield). ^1H NMR (400 MHz, CD_2Cl_2, 298.0 K): $\delta=8.48$ (s, 1H), 7.99 (dd, $J=8.3$, 1.5 Hz, 1H), 7.89 (d, $J=8.3$ Hz, 1H), 7.83 (dd, $J=6.5$, 2.8 Hz, 1H), 7.71 (dd, $J=5.8$, 1.8 Hz, 1H), 7.57–7.46 (m, 15H), 7.29–7.22 (m, 2H), 6.62 (s, 4H), 2.16 (s, 6H), 1.77 ppm (s, 12H); well-resolved ^{13}C NMR spectra could not be obtained for this compound, owing to its poor solubility; elemental analysis calcd (%) for $C_{49}H_{44}AuBNP$: C 66.45, H 5.01, N 1.58; found: C 66.37, H 4.98, N 1.55.

Synthesis of Pt-B: This Pt^{II} compound was prepared in a similar manner to **Au-B**, by using [*trans*-$Pt(PPh_3)_2Cl_2$] (108 mg, 0.14 mmol), **B1** (122 mg, 0.28 mmol), CuI (2 mg), and Et_3N (6 mL) in degassed CH_2Cl_2 (30 mL). After the completion of the reaction, the mixture was purified by column chromatography on silica gel (hexanes/CH_2Cl_2, 4:1) to give **Pt-B** as a light-yellow powder (62% yield). ^1H NMR (400 MHz, C_6D_6, 298.0 K): $\delta=8.22$ (s, 1H), 8.00 (d, $J=7.3$ Hz, 1H), 7.85 (dd, $J=12.8$, 6.8 Hz, 6H), 7.41 (d, $J=7.6$ Hz, 1H), 7.11–6.93 (m, 11H), 6.88 (d, $J=8.3$ Hz, 1H), 6.77 (s, 4H), 6.66 (dd, $J=8.3$, 1.5 Hz, 1H), 2.23 (s, 6H), 1.94 ppm (s, 12H); $^{13}C\{^1H\}$ NMR (100 MHz, $CDCl_3$): $\delta=155.4$, 147.2, 146.2, 142.8, 140.5, 135.7, 135.4, 135.3, 135.2, 134.1, 131.3, 131.1, 131.0, 130.7, 130.3, 128.6, 128.5, 128.4, 125.6, 121.7, 117.0, 25.2, 20.9 ppm; elemental analysis calcd (%) for $C_{98}H_{88}PtB_2N_2P_2$: C 74.86, H 5.64, N 1.78; found: C 73.65, H 6.28, N 2.36.

X-ray diffraction analysis: Single crystals of all three metal compounds were mounted onto glass fibers and the data were collected on a Bruker Apex II single-crystal X-ray diffractometer with graphite-monochromated Mo Kα radiation, operating at 50 kV and 30 mA at 180 K. The data were processed on a PC with the aid of the Bruker SHELXTL software package (version 6.14)[16] and corrected for absorption effects. The structures were solved by using direct methods. All non-hydrogen atoms were refined anisotropically. Disordered CH_2Cl_2 solvent molecules were located in the crystal lattice of **Au-B** (1.5 CH_2Cl_2 molecules per molecule of **Au-B**) and were modeled and refined successfully. $CHCl_3$ solvent molecules were located in the crystal lattice of **Re-B** (2 $CHCl_3$ molecules per molecule of **Re-B**) and were refined successfully. Benzene solvent molecules were located in the crystal lattice of **Pt-B** (5 C_6H_6 molecules per molecule of **Pt-B**) and were refined successfully. The Pt atom in **Pt-B** was located at a crystallographically imposed inversion center. The positions of all hydrogen atoms were calculated and their contributions were included in structure-factor calculations. CCDC-908883 (**Re-B**), CCDC-908884 (**Pt-B**), and CCDC-908885 (**Au-B**) contain the supplementary crystallographic data for this paper. These data can be obtained free of charge from The Cambridge Crystallographic Data Centre via www.ccdc.cam.ac.uk/data_request/cif.

Molecular calculations: The computational calculations were performed by using Gaussian 09, revision B.0[17] software package and the High Performance Computing Virtual Laboratory (HPCVL) at Queen's University. The ground-state geometries were fully optimized at the B3LYP[18] level by using the LANL2DZ basis set for metal atoms and the 6–31G(d) basis set for all other atoms.[19] The initial geometric parameters in the calculations were employed from crystal-structure data for geometry optimization. Time-dependent density function theory (TD-DFT) calculations were performed to obtain the vertical singlet energies and triplet excitation energies.

Acknowledgements

We thank the Natural Sciences and Engineering Research Council for financial support. S.W. thanks the Canada Council for the Arts for a Killam Research Fellowship.

---

[1] a) Y. L. Rao, H. Amarne, S. B. Zhao, T. M. McCormick, S. Martic, Y. Sun, R. Wang, S. Wang, *J. Am. Chem. Soc.* **2008**, *130*, 12898; b) C. Baik, Z. M. Hudson, H. Amarne, S. Wang, *J. Am. Chem. Soc.* **2009**, *131*, 14549; c) C. Baik, S. K. Murphy, S. Wang, *Angew. Chem.* **2010**, *122*, 8400; *Angew. Chem. Int. Ed.* **2010**, *49*, 8224; d) H. Amarne, C. Baik, S. K. Murphy, S. Wang, *Chem. Eur. J.* **2010**, *16*, 4750; e) S. K. Murphy, C. Baik, J. S. Lu, S. Wang, *Org. Lett.* **2010**, *12*, 5266; f) H. Amarne, C. Baik, R. Wang, S. Wang, *Organometallics* **2011**, *30*, 665; g) Y. L. Rao, S. Wang, *Organometallics* **2011**, *30*, 4453.

[2] Y. L. Rao, H. Amarne, S. Wang, *Coord. Chem. Rev.* **2012**, *256*, 759, and references therein.

[3] Y. L. Rao, H. Amarne, S. Wang, *Dalton Trans.* **2013**, *42*, 638.

[4] Z. M. Hudson, S. B. Ko, S. Yamaguchi, S. Wang, *Org. Lett.* **2012**, *14*, 5610.

[5] a) G. Berkovic, V. Krongauz, V. Weiss, *Chem. Rev.* **2000**, *100*, 1741; b) S. Kobatake, M. Irie, *Annu. Rep. Prog. Chem. Sect. C* **2003**, *99*, 277; c) M. Irie, *Chem. Rev.* **2000**, *100*, 1685; d) J. C. Crano, R. J. Guglielmetti, in *Organic Photochromic and Thermochromic Compounds*, Plenum, New York (USA), **1999**; e) C.-C. Ko, V. W. W. Yam, *J. Mater. Chem.* **2010**, *20*, 2063, and references therein; f) S. Kume, H. Nishihara, *Dalton Trans.* **2008**, 3260; g) R. Sakamoto, S. Kume, M. Sugimoto, H. Nishihara, *Chem. Eur. J.* **2009**, *15*, 1429; h) B. L. Feringa, in *Molecular Switches*, Wiley-VCH, Weinheim (Germany), **2001**; i) V. Aubert, V. Guerchais, E. Ishow, K. Hoang-Thi, I. Ledoux, K. Nakatani, H. Le Bozec, *Angew. Chem.* **2008**, *120*, 587; *Angew. Chem. Int. Ed.* **2008**, *47*, 577; j) J. Areephong, H. Logtenberg, W. R. Browne, B. L. Feringa, *Org. Lett.* **2010**, *12*, 2132.

[6] a) N. Tamai, H. Miyasaka, *Chem. Rev.* **2000**, *100*, 1875 and references therein; b) E. Deniz, M. Battal, J. Cusido, S. Sortino, F. M. Raymo, *Phys. Chem. Chem. Phys.* **2012**, *14*, 10300.

[7] a) M. T. Indelli, S. Carli, M. Ghirotti, C. Chiorboli, M. Ravaglia, M. Garavelli, F. Scandola, *J. Am. Chem. Soc.* **2008**, *130*, 7286; b) V. W.-W. Yam, C. C. Ko, N. Zhu, *J. Am. Chem. Soc.* **2004**, *126*, 12734; c) M. N. Roberts, J. K. Nagle, J. G. Finden, N. R. Branda, M. O. Wolf, *Inorg. Chem.* **2009**, *48*, 19.

[8] V. W.-W. Yam, V. C.-Y. Lau, K. K. Cheung, *Organometallics* **1995**, *14*, 2749.

[9] a) S.-T. Lam, N. Zhu, V. W.-W. Yam, *Inorg. Chem.* **2009**, *48*, 9664; b) M. S. Khan, A. K. Kakkar, N. J. Long, J. Lewis, P. Raithby, P. Nguyen, T. B. Marder, F. Wittmann, R. H. Friend, *J. Mater. Chem.* **1994**, *4*, 1227; c) K. Sonogashira, S. Takahashi, N. Hagihara, *Macromolecules* **1977**, *10*, 879; d) S. Takahashi, M. Kariya, T. Yakate, K. Sonogashira, N. Hagihara, *Macromolecules* **1978**, *11*, 1063.

[10] a) L. F. Elmuti, R. A. Peebles, S. A. Peebles, A. L. Steber, J. L. Neill, B. H. Pate, *Phys. Chem. Chem. Phys.* **2011**, *13*, 14043; b) M. Nishio, *Phys. Chem. Chem. Phys.* **2011**, *13*, 13873, and references therein.

[11] a) V. W.-W. Yam, *Chem. Commun.* **2001**, 789; b) M. Wrighton, D. L. Morse, *J. Am. Chem. Soc.* **1974**, *96*, 998; c) A. S. Polo, M. K. Itokazu, K. M. Frin, A. O. de T. Patrocínio, N. Y. M. Iha, *Coord. Chem. Rev.* **2006**, *250*, 1669; d) V. W.-W. Yam, Y. Yang, J. Zhang, B. W. K. Chu, N. Zhu, *Organometallics* **2001**, *20*, 4911; e) M. K. Itokazu, A. S. Polo, N. Y. M. Iha, *J. Photochem. Photobiol. A* **2003**, *160*, 27.

[12] a) V. W. W. Yam, S. W. K. Choi, *J. Chem. Soc. Dalton Trans.* **1996**, 4227; b) V. W. W. Yam, S. W. K. Choi, K. K. Cheung, *J. Chem. Soc. Dalton Trans.* **1996**, 3411; c) V. W. W. Yam, K. K. Cheung, S. K. Yip, K. K. Cheung, *J. Organomet. Chem.* **2003**, *681*, 196.

[13] a) Z. M. Hudson, C. Sun, K. J. Harris, B. E. G. Lucier, R. W. Schurko, S. Wang, *Inorg. Chem.* **2011**, *50*, 3447; b) P. R. Zhang, D. J. Berg, R. H. Mitchell, B. Patrick, *Organometallics* **2012**, *31*, 8121; c) K. Haskins-Glusac, I. Ghiviriga, K. A. Abboud, K. S. Schanze, *J. Phys. Chem. B* **2004**, *108*, 4969.

[14] a) T. Sajoto, P. I. Djurovich, A. B. Tamayo, J. Oxgaard, W. A. Goddard, M. E. Thompson, *J. Am. Chem. Soc.* **2009**, *131*, 9813; b) G. A. Crosby, N. J. Demas, *J. Am. Chem. Soc.* **1970**, *92*, 7262.
[15] a) D. Abdallah, J. Whelan, J. M. Dust, S. Hoz, E. Buncel, *J. Phys. Chem. A* **2009**, *113*, 6640; b) C. A. Parker, *Proc. R. Soc. London Ser. A* **1953**, *220*, 104.
[16] SHELXTL Version 6.14, Bruker AXS, **2000–2003**.
[17] Gaussian 09, Revision B.01, M. J. Frisch, G. W. Trucks, H. B. Schlegel, G. E. Scuseria, M. A. Robb, J. R. Cheeseman, G. Scalmani, V. Barone, B. Mennucci, G. A. Petersson, H. Nakatsuji, M. Caricato, X. Li, H. P. Hratchian, A. F. Izmaylov, J. Bloino, G. Zheng, J. L. Sonnenberg, M. Hada, M. Ehara, K. Toyota, R. Fukuda, J. Hasegawa, M. Ishida, T. Nakajima, Y. Honda, O. Kitao, H. Nakai, T. Vreven, J. A. Montgomery, Jr., J. E. Peralta, F. Ogliaro, M. Bearpark, J. J. Heyd, E. Brothers, K. N. Kudin, V. N. Staroverov, T. Keith, R. Kobayashi, J. Normand, K. Raghavachari, A. Rendell, J. C. Burant, S. S. Iyengar, J. Tomasi, M. Cossi, N. Rega, J. M. Millam, M. Klene, J. E. Knox, J. B. Cross, V. Bakken, C. Adamo, J. Jaramillo, R. Gomperts, R. E. Stratmann, O. Yazyev, A. J. Austin, R. Cammi, C. Pomelli, J. W. Ochterski, R. L. Martin, K. Morokuma, V. G. Zakrzewski, G. A. Voth, P. Salvador, J. J. Dannenberg, S. Dapprich, A. D. Daniels, O. Farkas, J. B. Foresman, J. V. Ortiz, J. Cioslowski, and D. J. Fox, Gaussian, Inc., Wallingford CT, **2010**.
[18] a) A. D. Becke, *J. Chem. Phys.* **1993**, *98*, 5648; b) C. Lee, C. W. Yang, R. G. Parr, *Phys. Rev. B* **1988**, *37*, 785.
[19] P. J. Hay, *J. Phys. Chem. A* **2002**, *106*, 1634.

Received: November 13, 2012